



**HAL**  
open science

# Diverging seasonal extremes for ocean acidification during the twenty-first century

Lester Kwiatkowski, James C. Orr

► **To cite this version:**

Lester Kwiatkowski, James C. Orr. Diverging seasonal extremes for ocean acidification during the twenty-first century. *Nature Climate Change*, 2018, 8 (2), pp.141-145. 10.1038/s41558-017-0054-0 . hal-02044904

**HAL Id: hal-02044904**

**<https://hal.science/hal-02044904v1>**

Submitted on 5 Mar 2019

**HAL** is a multi-disciplinary open access archive for the deposit and dissemination of scientific research documents, whether they are published or not. The documents may come from teaching and research institutions in France or abroad, or from public or private research centers.

L'archive ouverte pluridisciplinaire **HAL**, est destinée au dépôt et à la diffusion de documents scientifiques de niveau recherche, publiés ou non, émanant des établissements d'enseignement et de recherche français ou étrangers, des laboratoires publics ou privés.

# Diverging seasonal extremes for ocean acidification during the twenty-first century

Lester Kwiatkowski<sup>1\*</sup>, James Orr<sup>1</sup>

Laboratoire des Sciences du Climat et de l'Environnement (LSCE), IPSL, CEA/CNRS/UVSQ, Orme des Merisiers, Gif-sur-Yvette, 91190, France.

\*Lester Kwiatkowski

Laboratoire des Sciences du Climat et de l'Environnement (LSCE)

Orme des Merisiers

Gif-sur-Yvette

91190

France

Lester.Kwiatkowski@lsce.ipsl.fr

How ocean acidification will affect marine organisms depends on changes in both the long-term mean and the short-term temporal variability of carbonate chemistry<sup>1,2,3,4,5,6,7,8</sup>.

While the decadal-to-centennial response to atmospheric CO<sub>2</sub> and climate change is constrained by observations and models<sup>1,9</sup>, little is known about corresponding changes in seasonality<sup>10,11,12</sup>, particularly for pH. Here we assess the latter by analysing 9 Earth System Models (ESMs) forced with a business-as-usual emissions scenario<sup>13</sup>. During the twenty-first century, the seasonal cycle of surface-ocean pH was attenuated by 16±7 %, on average, while that for hydrogen ion concentration [H<sup>+</sup>] was amplified by 81±16 %. Simultaneously, the seasonal amplitude of aragonite saturation state ( $\Omega_{\text{arag}}$ ) was attenuated except in the subtropics where it was amplified. These contrasting changes derive from regionally varying sensitivities of these variables to atmospheric CO<sub>2</sub> and climate change and diverging trends in seasonal extremes in the primary controlling variables (temperature, dissolved inorganic carbon, and alkalinity). Projected seasonality changes will tend to exacerbate impacts of increasing [H<sup>+</sup>] on marine organisms during summer and ameliorate impacts during winter, although the opposite holds in the high latitudes. Similarly over most of the ocean, impacts from declining  $\Omega_{\text{arag}}$  are likely to be intensified during summer and dampened during winter.

45 Ocean CO<sub>2</sub> uptake affects marine chemistry via ocean acidification<sup>1,9,14</sup>, a process that  
46 increases concentrations of CO<sub>2</sub>, H<sup>+</sup> and HCO<sub>3</sub><sup>-</sup>, and reduces levels of pH and CO<sub>3</sub><sup>2-</sup>. Although  
47 much effort has been devoted to assessing the direct and indirect effects of increasing  
48 atmospheric CO<sub>2</sub> on the mean state of these ocean carbonate chemistry variables, few  
49 studies have addressed the corresponding changes in their seasonal cycles<sup>10,11,12</sup>.

50  
51 The seasonal cycles of ocean carbonate chemistry variables are the result of variations in the  
52 seasonality of different physical and biological processes<sup>6,7</sup>. Those for pCO<sub>2</sub> and pH are  
53 largely regulated by variations in temperature in the subtropics, while at higher latitudes  
54 their oscillations are typically dominated by biological uptake and release of CO<sub>2</sub>  
55 (photosynthesis and respiration). In contrast, temperature plays a minor role in controlling  
56 the seasonal cycles of the carbonate saturation state of seawater ( $\Omega = [Ca^{2+}][CO_3^{2-}]/K_{sp}$ )  
57 even at lower latitudes; rather, it is the variability of total alkalinity and dissolved inorganic  
58 carbon that dominates<sup>6,7</sup>.

59  
60 To survive, marine organisms must cope with variations in their local environment, however  
61 many may be highly sensitive to changes in ocean carbonate chemistry<sup>15,16</sup>. Calcifying  
62 species such as echinoderms, byozoans and cnidarians exhibit depressed calcification,  
63 growth and survival rates at lower  $\Omega_{arag/calc}$  (refs. <sup>3,4,15</sup>). In teleost fish and marine  
64 invertebrates, ion exchange is reduced by extracellular acidosis or high external [H<sup>+</sup>],  
65 depressing protein synthesis and metabolic rates<sup>17</sup>. Physiological and behavioural  
66 functioning is also sensitive to pCO<sub>2</sub>, with high external concentrations impairing olfactory  
67 discrimination<sup>18</sup> and predator-prey responses<sup>19</sup>.

68  
69 Accounting for seasonal variability in carbonate chemistry influences the timing of the  
70 projected onset of CaCO<sub>3</sub> undersaturation<sup>10,11,20</sup>, when waters become corrosive to pure  
71 aragonite ( $\Omega_{arag} < 1$ ) and calcite ( $\Omega_{calc} < 1$ ) (i.e., metastable and stable forms of CaCO<sub>3</sub>). These  
72 seasonal variations also affect when surface waters will reach a proposed threshold, beyond  
73 which pCO<sub>2</sub> levels may become damaging<sup>12</sup>. Here we explore how seasonality of surface-  
74 ocean [H<sup>+</sup>], pH and  $\Omega_{arag}$  will respond to projected increases of atmospheric CO<sub>2</sub> and climate  
75 change during the twenty-first century. Unlike studies that have assumed unchanging  
76 seasonality, combining observational estimates of present seasonality (repeated in time)  
77 with model projections of the change in mean state<sup>10,11</sup>, we use an ensemble of 9 Earth  
78 System Models (ESMs) containing coupled ocean biogeochemistry schemes. Thus we assess  
79 how seasonality is affected by increasing concentrations of atmospheric CO<sub>2</sub> and climate-  
80 change driven changes in sea surface temperature and biology<sup>9,21</sup>.

81  
82 Ocean biogeochemistry models (OBM) generally reproduce the amplitude and phase of  
83 observational estimates for seasonal air-sea CO<sub>2</sub> fluxes in the Pacific<sup>22</sup>, Atlantic<sup>23</sup> and Indian  
84 Oceans<sup>24</sup> while their skill in high latitude regions is more limited<sup>23,25,26</sup>. We found consistent  
85 results for the CMIP5 ESMs that include an OBM. The models broadly capture the zonal-  
86 mean patterns of seasonal changes in [H<sup>+</sup>] ( $r \sim 0.8$ ) and  $\Omega_{arag}$  ( $r \sim 0.95$ ) of observational  
87 climatologies (Supplementary Figs. 1-6). Hence they appear to offer the best option to assess  
88 projected changes in seasonality during the coming century. Nonetheless, model  
89 performance in the Southern Ocean is particularly limited, with certain models negatively  
90 correlated with the [H<sup>+</sup>] climatology, possibly due to excessive simulated warming in

91 summer<sup>25</sup> or underestimated winter convective CO<sub>2</sub> entrainment and the impact of  
92 biological CO<sub>2</sub> uptake<sup>26</sup>.

93  
94 Projected trends in seasonality were evaluated for the business-as-usual (2006-2100)  
95 Representative Concentration Pathway 8.5 (RCP8.5)<sup>13</sup> relative to results from the historical  
96 simulation<sup>27</sup> (1990-1999). Changes in seasonality were determined by subtracting a cubic  
97 spline fit from the monthly time series in each grid cell and calculating the annual peak-to-  
98 peak amplitude for each year of the detrended dataset. Both the mean state and seasonality  
99 of projected [H<sup>+</sup>], pH and Ω<sub>arag</sub> change over the twenty-first century, as illustrated in Figure 1  
100 for one model.

101  
102 During this century, the amplitude of seasonal cycle in [H<sup>+</sup>] is projected to increase by 81±16  
103 % (multi-model mean ± 1SD) (Fig. 2a). Increases in seasonal amplitudes of [H<sup>+</sup>] are generally  
104 higher in the high latitudes, particularly in the Arctic where the average amplification is  
105 147±57 % (Fig. 3a, S8). Yet unlike the seasonal amplitude for [H<sup>+</sup>], that for pH is projected to  
106 decline globally, on average by 16±7 % during the twenty-first century (Fig.2b). Attenuation  
107 is generally more intense in the low and mid-latitudes but also occurs over most of the high-  
108 latitude ocean (Fig. 3b, S8). Given that pH is directly related to [H<sup>+</sup>], it is counterintuitive that  
109 while the seasonal amplitude in [H<sup>+</sup>] increases, the seasonal amplitude in pH declines.  
110 However, the log transformation implies that

$$111 \quad d \text{pH} = \frac{-1}{2.303} \frac{d[\text{H}^+]}{[\text{H}^+]} \quad (1)$$

112 That is, the seasonal amplitude of pH depends not only on the seasonal amplitude of [H<sup>+</sup>] but  
113 also on the annual mean [H<sup>+</sup>]. For the seasonal amplitude in pH to remain constant in time,  
114 the relative change in the seasonal amplitude of [H<sup>+</sup>] would have to equal the relative  
115 change in annual mean [H<sup>+</sup>]. Although the CMIP5 models project that the global mean,  
116 seasonal amplitude of [H<sup>+</sup>] increases by 81±16 % over the twenty-first century, the annual  
117 global mean [H<sup>+</sup>] simultaneously increases by 117±3 %. Hence their combination results in  
118 reduced seasonal amplitude of pH. In contrast, in the parts of the Arctic and Southern Ocean  
119 that exhibit increases in the seasonal amplitude of pH, the relative change in the seasonal  
120 amplitude of [H<sup>+</sup>] is larger than the relative change in the [H<sup>+</sup>] mean state. Yet in those  
121 regions, there is less agreement among models about the sign of these changes (Figs. 3b,  
122 S8).

123  
124 Regarding Ω<sub>arag</sub>, its global average seasonal amplitude is attenuated by 9±8 % during the  
125 twenty-first century (Fig. 3c). Attenuation can exceed 40 % in the temperate-to-polar zones,  
126 while in the subtropics, where the amplitude of the seasonal cycle of Ω<sub>arag</sub> is much smaller  
127 (Supplementary Fig. 7), there is amplification of up to 30 % (Fig. 3c), as discussed below.  
128 These projected changes in the seasonal amplitude of [H<sup>+</sup>], pH and Ω<sub>arag</sub> result from  
129 nonidentical changes in both the seasonal maxima and minima (Fig. 1, S12).

130  
131 To further investigate the causes of changes in seasonal amplitudes of derived variables [H<sup>+</sup>]  
132 and Ω<sub>arag</sub>, we used 2 complementary approaches: (1) idealised simulations and (2) first-order  
133 Taylor-series deconvolution. The idealised simulations partition the geochemical versus  
134 radiative effects of increasing atmospheric CO<sub>2</sub>, where the geochemical effect is due to

135 ocean carbon uptake and the radiative effect influences carbonate chemistry through rising  
 136 temperatures and simultaneous changes in marine biological activity. The deconvolution  
 137 quantifies how the seasonal amplitude of each derived variable ( $\Delta y$ ), is affected by changes  
 138 in temperature (T), salinity (S), dissolved inorganic carbon ( $C_T$ ) and total alkalinity ( $A_T$ ), i.e.,  
 139 four model variables used to calculate carbonate chemistry. That is for  $y = f(C_T, A_T, T, S)$ ,

$$\Delta y = \left(\frac{\partial y}{\partial C_T}\right) \Delta C_T + \left(\frac{\partial y}{\partial A_T}\right) \Delta A_T + \left(\frac{\partial y}{\partial T}\right) \Delta T + \left(\frac{\partial y}{\partial S}\right) \Delta S \quad (2)$$

141  
 142 where the partial differentials are estimated numerically and  $\Delta T$ ,  $\Delta C_T$ ,  $\Delta A_T$  and  $\Delta S$  are the  
 143 changes in input variables, synchronous with  $\Delta y$ , assuming other contributions are negligible.  
 144 For the change in amplitude, Equation (2) is evaluated separately with decadal mean  
 145 seasonal cycles for the first and last simulated decades of the RCP8.5 scenario, and then the  
 146 latter is subtracted from the former.

147  
 148 This deconvolution illustrates how the proximate drivers of seasonal amplification of  $[H^+]$   
 149 vary spatially. In the mid-to-high latitudes it is the residual effect of opposing increases in the  
 150 terms for dissolved inorganic carbon ( $(\partial H^+/\partial C_T)\Delta C_T$ ) and total alkalinity ( $(\partial H^+/\partial A_T)\Delta A_T$ ) that  
 151 dominates. However, in the low latitudes, changes in these two terms largely compensate,  
 152 so it is the increase in the temperature term ( $(\partial H^+/\partial T)\Delta T$ ) that dominates (Supplementary  
 153 Fig. 9). Because the sensitivities of  $H^+$  to  $C_T$  and  $A_T$  (partial differentials) are roughly equal and  
 154 opposite, it is the balance between  $\Delta C_T$  and  $\Delta A_T$  that control the change in seasonal  
 155 amplitude of  $[H^+]$  in the mid-to high latitudes (Supplementary Fig. 10). One cannot assume  
 156 that  $\Delta A_T$  remains constant while only  $\Delta C_T$  will change. For instance, changes in  $\Delta A_T$  will be  
 157 decoupled from those of  $\Delta C_T$  due to an altered hydrological cycle. Increased freshwater  
 158 input dilutes  $C_T$  and  $A_T$ , but  $C_T$  then tends to equilibrate with atmospheric  $CO_2$ , unlike  $A_T$ .  
 159 Hence addition of low alkalinity freshwater reduces pH, despite the opposite tendency from  
 160 dilution alone. The high latitudes will experience this effect most, from enhanced  
 161 precipitation, ice melt, and river runoff. Decoupling will also result from anthropogenic  $CO_2$   
 162 invasion and changes in primary production. In the low latitudes, while the  $C_T$  and  $A_T$  terms  
 163 are small and compensating, the temperature term dominates, enhanced by a doubling of  
 164  $\partial H^+/\partial T$  (Supplementary Fig. 11). The ultimate drivers of this seasonal amplification in  $[H^+]$  are  
 165 demonstrated by the idealised simulations, which show that it is the geochemical effect of  
 166 increasing atmospheric  $CO_2$  and consequently reduced buffer capacity<sup>29,30</sup> that is responsible  
 167 for 92 % of global amplification, while the radiative effect provides minor reinforcement (Fig.  
 168 4, S13).

169  
 170 For  $\Omega_{arag}$ , the proximate drivers of the general attenuation of its seasonal amplitude are a  
 171 decline in the  $C_T$  term ( $(\partial \Omega_{arag}/\partial C_T)\Delta C_T$ ) which typically outweighs an opposing increase in the  
 172  $A_T$  term ( $(\partial \Omega_{arag}/\partial A_T)\Delta A_T$ ) (Supplementary Figs. 9-10). In the subtropics though, there is little  
 173 change in the  $A_T$  term, while the  $C_T$  term increases due to a larger change in  $\Delta C_T$ , driving  
 174 amplification of the  $\Omega_{arag}$  seasonal cycle in these regions. The ultimate driver of the seasonal  
 175 attenuation in  $\Omega_{arag}$  is the geochemical effect of increasing atmospheric  $CO_2$  which is  
 176 responsible for >100 % of global attenuation, being partly offset by the radiative effect (Fig.  
 177 4, S13). In contrast, the subtropical amplification of the seasonal cycle of  $\Omega_{arag}$  results from  
 178 the radiative effect driving enhanced amplification over the low latitudes in combination  
 179 with the weaker attenuation from the geochemical effect in the subtropics.

180

181 We have shown that under a business-as-usual emissions scenario, the seasonal variability of  
182 ocean carbonate chemistry is projected to change substantially during this century. Despite  
183 the diversity of OBMs in the multi-model ensemble<sup>9,21</sup>, spatial patterns of the change in  
184 seasonal amplitude of  $[H^+]$ , pH, and  $\Omega_{arag}$  are generally consistent (Fig. 3, S8). Previously it  
185 was shown that increasing atmospheric  $CO_2$  will amplify the seasonal cycle of surface-ocean  
186  $pCO_2$  (ref. <sup>12</sup>), potentially resulting in earlier exposure to detrimental  $pCO_2$  conditions for  
187 marine organisms. Here we show that increasing atmospheric  $CO_2$  must also amplify the  
188 seasonal cycle of  $[H^+]$  in a similar manner. This is consistent with the near-linear relationship  
189 between  $[H^+]$  and  $pCO_2$  for annual-mean trends during the twenty-first century<sup>31</sup>.

190

191 Amplified  $[H^+]$  seasonality may worsen impacts from the long-term mean increase in  $[H^+]$ ,  
192 potentially resulting in earlier seasonal exposure to conditions that cause physiological  
193 acidosis and depress protein synthesis and metabolic rates in marine organisms. In the low  
194 latitudes, this enhanced exposure is most likely to occur during summer when warming  
195 drives the  $[H^+]$  seasonal high. In the high latitudes, enhanced exposure is most likely to occur  
196 when the effect of photosynthesis on  $[H^+]$  drawdown is limited<sup>6,7</sup>. But amplified  $[H^+]$   
197 seasonality will also diminish exposure to conditions that cause acidosis during seasonal  
198 lows, e.g., in winter months in the low-latitudes and during phytoplankton blooms in the  
199 high-latitudes.

200

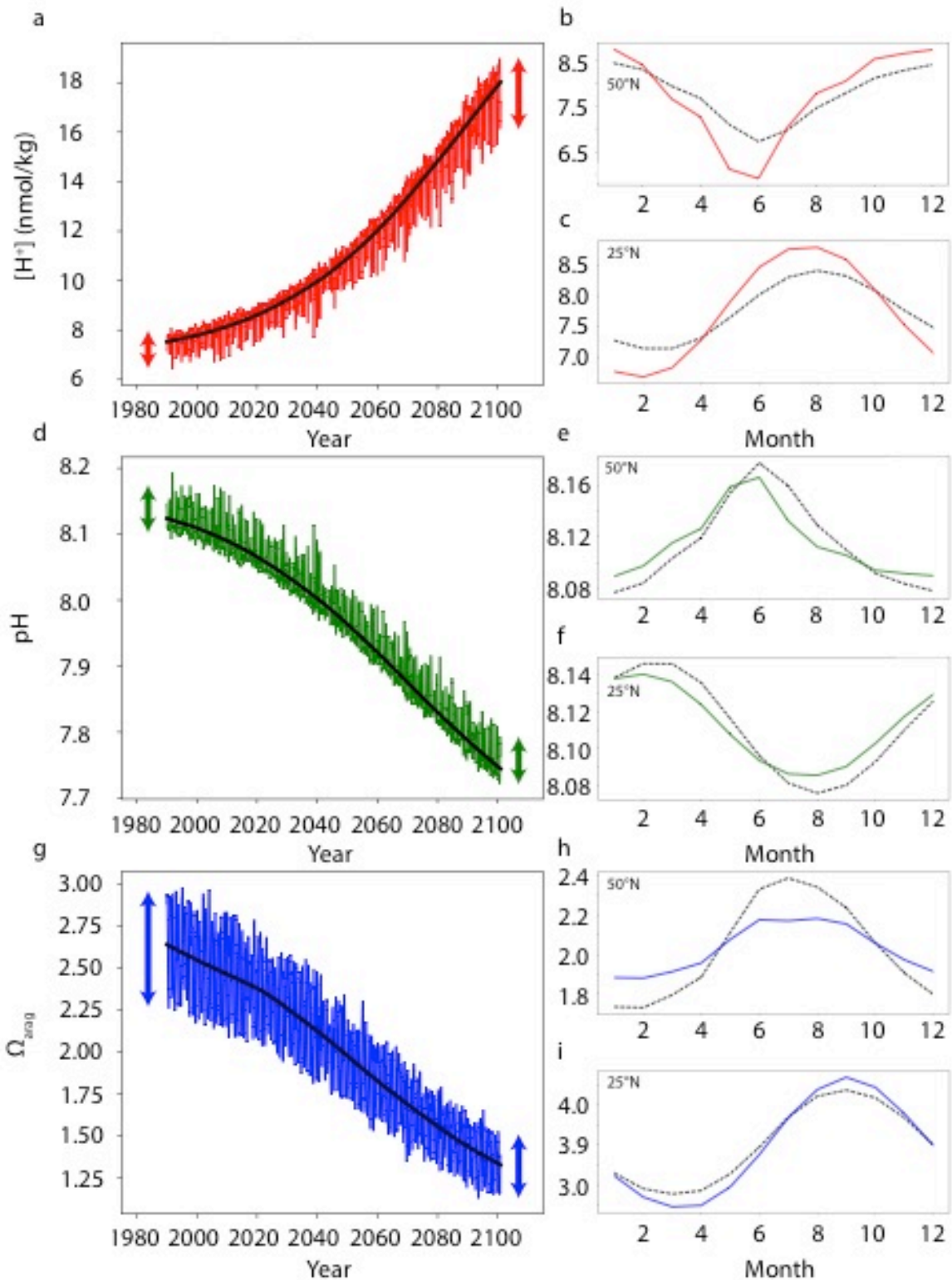
201 The seasonal amplitude of  $\Omega_{arag}$  is projected to amplify in some regions and attenuate in  
202 others. Attenuation dominates throughout most of the ocean owing to increases in aqueous  
203 carbon dioxide  $[CO_2^*]$ , which reduces carbonate ion  $[CO_3^{2-}]$  and hence the buffer capacity. In  
204 the subtropics though, the seasonal amplitude of  $\Omega_{arag}$  increases because amplification  
205 driven by the radiative effect of  $CO_2$  dominates the locally weak geochemical effect. The  
206 general attenuation of the seasonal amplitude of  $\Omega_{arag}$  is likely to exacerbate the impact of  
207 declining  $\Omega_{arag}$  during the summer high while dampening the impact of declining  $\Omega_{arag}$  during  
208 the winter low.

209

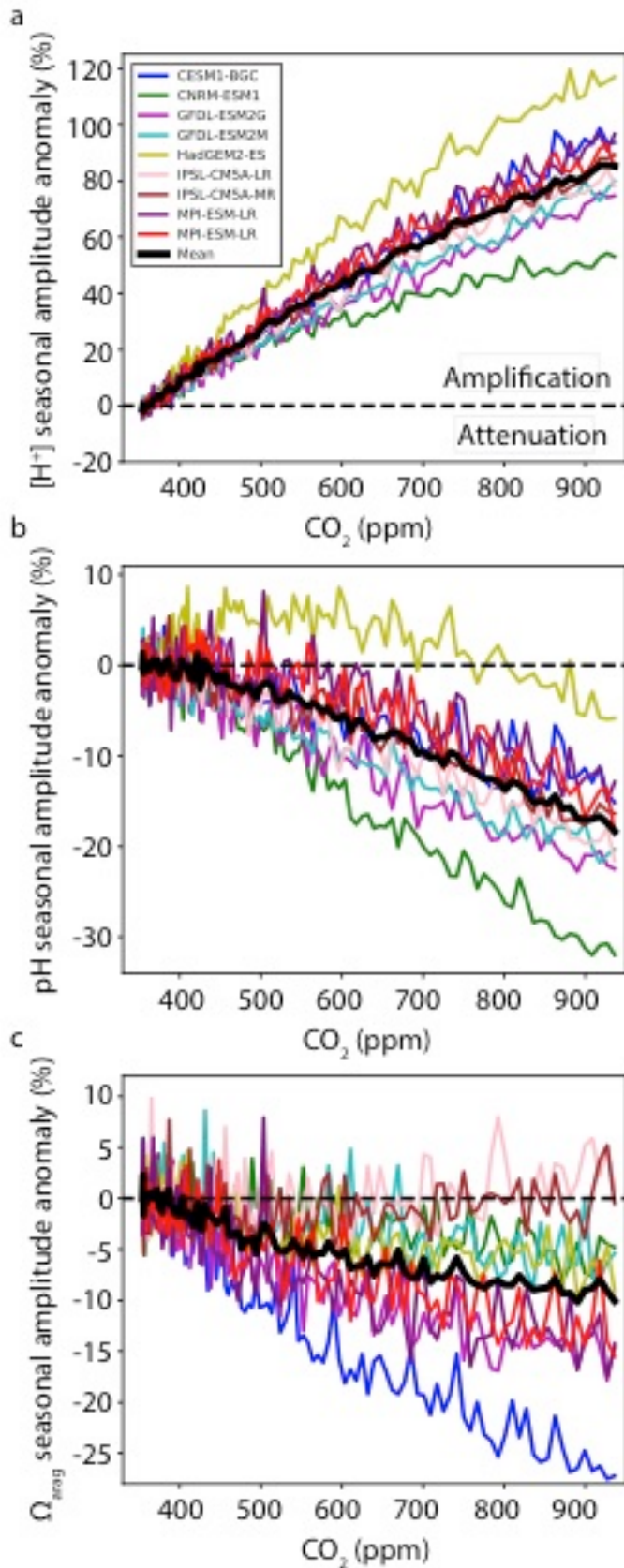
210 The same processes that will affect future seasonal variability, particularly the direct  
211 geochemical effect from the atmospheric  $CO_2$  increase and the corresponding indirect effect  
212 from radiative warming, are likely to affect future diurnal variability. Indeed we estimate an  
213 amplification of the diurnal cycle of  $[H^+]$  (122%) and an attenuation of the diurnal cycle of  
214  $\Omega_{arag}$  (20%) that are similar to our estimates for the seasonal cycle, based on differences in  
215 observations of diel pH variability reported for two adjacent sites in the Bay of Naples, a  
216 control station and a station where natural venting of pure  $CO_2$  has perturbed oceanic  $pCO_2$   
217 to reach levels expected for the late twenty-first century (Table S2; ref. <sup>32</sup>). Future research  
218 should assess how altered carbonate chemistry variability on both diurnal<sup>33,34</sup> and seasonal  
219 timescales will affect marine organisms, especially those suspected to be vulnerable to  
220 ocean acidification.

221

222 The diversity in projected changes in seasonal extremes of  $[H^+]$ , pH,  $\Omega_{arag}$  and  $pCO_2$   
223 emphasizes the need to improve our understanding of the mechanisms that control how  
224 specific marine organisms are affected by ocean acidification. In particular, we will need to  
225 study the sensitivity of marine organisms to these simultaneous yet contrasting changes in  
226 seasonality to be able to assess aggregate effects on marine communities.



229  
230 **Figure 1. Changing seasonal cycles of carbonate chemistry variables.** The projected **a-c**,  $[H^+]$   
231 **d-f**, pH and **g-i**,  $\Omega_{arag}$  under the historical and RCP8.5 scenario of one CMIP5 model (MPI-  
232 ESM-LR). First column, monthly values and the long-term mean trend from an illustrative  
233 grid cell in the South Pacific ( $110^\circ W$ ,  $40^\circ S$ ). Second column, the detrended zonal-mean  
234 seasonal cycles in the periods 1990-1999 (dashed) and 2090-2099 (line) at  $25^\circ N$  and  $50^\circ N$ .

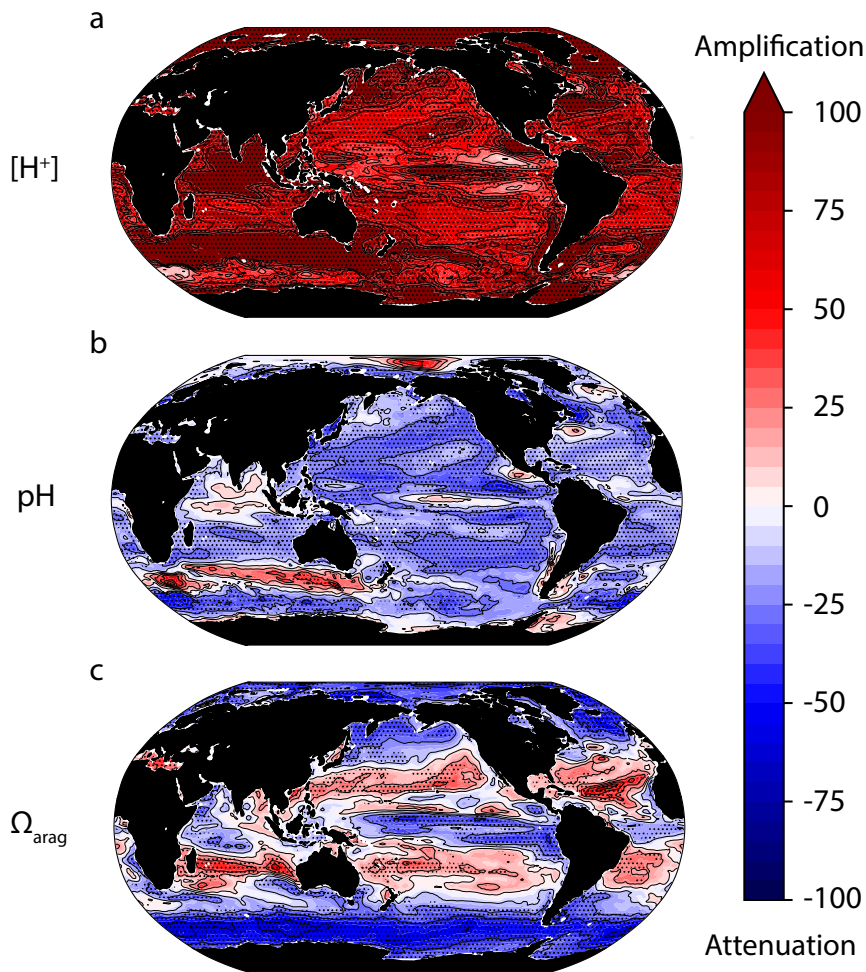


235  
 236  
 237  
 238

**Figure 2. Relative change in the seasonal amplitude of carbonate chemistry variables with rising atmospheric CO<sub>2</sub>.** Global anomaly in the seasonal amplitudes of a, [H<sup>+</sup>] b, pH and c, Ω<sub>arag</sub> relative to mean 1990s values as a function of atmospheric CO<sub>2</sub>.

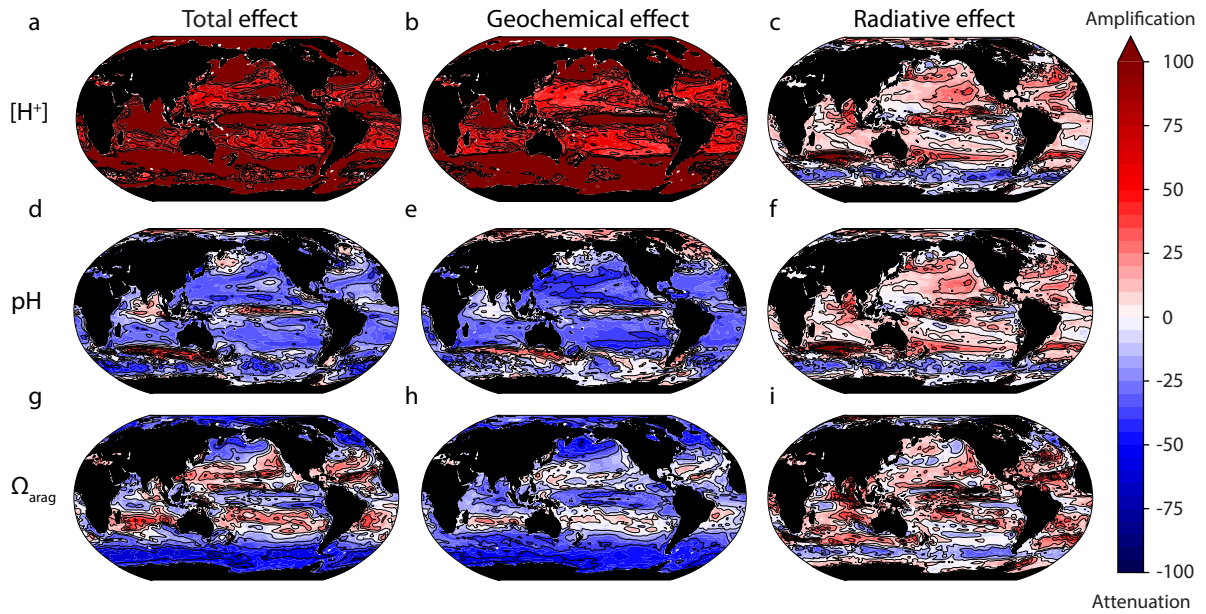


21<sup>st</sup> century change in seasonal amplitude (%)



239  
240  
241  
242  
243  
244  
245  
246  
247  
248  
249  
250  
251  
252  
253  
254  
255  
256  
257  
258

**Figure 3. The twenty-first century changes in seasonal amplitudes.** The model mean anomaly in the seasonal amplitude of **a**,  $[H^+]$  **b**, pH and **c**,  $\Omega_{arag}$  in the 2090s relative to the 1990s. Stippling shows areas of high confidence as determined by model sign agreement with a standard of 8 out of 9 models representing significance.



259  
 260 **Figure 4. Partitioning of geochemical and radiative effects of atmospheric CO<sub>2</sub> on**  
 261 **seasonality change.** The model mean anomaly (%) in the seasonal amplitudes of **a-c**, [H<sup>+</sup>], **d-**  
 262 **f**, pH and **g-i**, Ω<sub>arag</sub> due to the geochemical, radiative and combined effect of atmospheric  
 263 CO<sub>2</sub>. Anomalies are calculated for the last decade of 4xCO<sub>2</sub> simulations relative to the first  
 264 decade.

265  
 266  
 267  
 268  
 269  
 270  
 271  
 272  
 273  
 274  
 275  
 276  
 277  
 278  
 279  
 280  
 281  
 282  
 283  
 284  
 285  
 286  
 287  
 288  
 289  
 290

291 **References**

292

293 1. Orr, J. C. *et al.* Anthropogenic ocean acidification over the twenty-first century and its  
294 impact on calcifying organisms. *Nature* **437**, 681–686 (2005).

295 2. Wootton, J. T., Pfister, C. A. & Forester, J. D. Dynamic patterns and ecological impacts  
296 of declining ocean pH in a high-resolution multi-year dataset. *Proc. Natl. Acad. Sci.* **105**,  
297 18848–18853 (2008).

298 3. Albright, R. *et al.* Reversal of ocean acidification enhances net coral reef calcification.  
299 *Nature* **531**, 362–365 (2016).

300 4. Kwiatkowski, L. *et al.* Nighttime dissolution in a temperate coastal ocean ecosystem  
301 increases under acidification. *Sci. Rep.* **6**, 22984 (2016).

302 5. Shaw, E. C., McNeil, B. I., Tilbrook, B., Matear, R. & Bates, M. L. Anthropogenic  
303 changes to seawater buffer capacity combined with natural reef metabolism induce extreme  
304 future coral reef CO<sub>2</sub> conditions. *Glob. Change Biol.* **19**, 1632–1641 (2013).

305 6. Takahashi, T. *et al.* Climatological distributions of pH, pCO<sub>2</sub>, total CO<sub>2</sub>, alkalinity, and  
306 CaCO<sub>3</sub> saturation in the global surface ocean, and temporal changes at selected locations.  
307 *Mar. Chem.* **164**, 95–125 (2014).

308 7. Hagens, M. & Middelburg, J. J. Attributing seasonal pH variability in surface ocean  
309 waters to governing factors. *Geophys. Res. Lett.* **43**, 2016GL071719 (2016).

310 8. Takeshita, Y. *et al.* Including high-frequency variability in coastal ocean acidification  
311 projections. *Biogeosciences* **12**, 5853–5870 (2015).

312 9. Bopp, L. *et al.* Multiple stressors of ocean ecosystems in the 21st century: projections  
313 with CMIP5 models. *Biogeosciences* **10**, 6225–6245 (2013).

314 10. McNeil, B. I. & Matear, R. J. Southern Ocean acidification: A tipping point at 450-ppm  
315 atmospheric CO<sub>2</sub>. *Proc. Natl. Acad. Sci.* **105**, 18860–18864 (2008).

316 11. Sasse, T. P., McNeil, B. I., Matear, R. J. & Lenton, A. Quantifying the influence of CO<sub>2</sub>  
317 seasonality on future aragonite undersaturation onset. *Biogeosciences* **12**, 6017–6031  
318 (2015).

319 12. McNeil, B. I. & Sasse, T. P. Future ocean hypercapnia driven by anthropogenic  
320 amplification of the natural CO<sub>2</sub> cycle. *Nature* **529**, 383–386 (2016).

321 13. Riahi, K. *et al.* RCP 8.5—A scenario of comparatively high greenhouse gas emissions.  
322 *Clim. Change* **109**, 33–57 (2011).

323 14. Doney, S. C., Fabry, V. J., Feely, R. A. & Kleypas, J. A. Ocean Acidification: The Other  
324 CO<sub>2</sub> Problem. *Annu. Rev. Mar. Sci.* **1**, 169–192 (2009).

325 15. Kroeker, K. J., Kordas, R. L., Crim, R. N. & Singh, G. G. Meta-analysis reveals negative  
326 yet variable effects of ocean acidification on marine organisms. *Ecol. Lett.* **13**, 1419–1434  
327 (2010).

328 16. Mangan, S., Urbina, M. A., Findlay, H. S., Wilson, R. W. & Lewis, C. Fluctuating  
329 seawater pH/pCO<sub>2</sub> regimes are more energetically expensive than static pH/pCO<sub>2</sub> levels in  
330 the mussel *Mytilus edulis*. *Proc R Soc B* **284**, 20171642 (2017).

331 17. Pörtner, H.-O. Ecosystem effects of ocean acidification in times of ocean warming: a  
332 physiologists view. *Mar. Ecol. Prog. Ser.* **373**, 203–217 (2008).

333 18. Munday, P. L. *et al.* Ocean acidification impairs olfactory discrimination and homing  
334 ability of a marine fish. *Proc. Natl. Acad. Sci.* **106**, 1848–1852 (2009).

335 19. Watson, S.-A., Fields, J. B. & Munday, P. L. Ocean acidification alters predator  
336 behaviour and reduces predation rate. *Biol. Lett.* **13**, 20160797 (2017).

337 20. Gruber, N. *et al.* Rapid Progression of Ocean Acidification in the California Current

- 338 System. *Science* **337**, 220–223 (2012).
- 339 21. Kwiatkowski, L. *et al.* Emergent constraints on projections of declining primary  
340 production in the tropical oceans. *Nat. Clim. Change* **7**, 355–358 (2017).
- 341 22. Ishii, M. *et al.* Air–sea CO<sub>2</sub> flux in the Pacific Ocean for the period 1990–2009.  
342 *Biogeosciences* **11**, 709–734 (2014).
- 343 23. Schuster, U. *et al.* An assessment of the Atlantic and Arctic sea–air CO<sub>2</sub> fluxes, 1990–  
344 2009. *Biogeosciences* **10**, 607–627 (2013).
- 345 24. Sarma, V. V. S. S. *et al.* Sea–air CO<sub>2</sub> fluxes in the Indian Ocean between 1990 and  
346 2009. *Biogeosciences* **10**, 7035–7052 (2013).
- 347 25. Lenton, A. *et al.* Sea–air CO<sub>2</sub> fluxes in the Southern Ocean for the period  
348 1990–2009. *Biogeosciences* **10**, 4037–4054 (2013).
- 349 26. Mongwe, N. P., Chang, N. & Monteiro, P. M. S. The seasonal cycle as a mode to  
350 diagnose biases in modelled CO<sub>2</sub> fluxes in the Southern Ocean. *Ocean Model.* **106**, 90–103  
351 (2016).
- 352 27. Taylor, K. E., Stouffer, R. J. & Meehl, G. A. An Overview of CMIP5 and the Experiment  
353 Design. *Bull. Am. Meteorol. Soc.* **93**, 485–498 (2011).
- 354 28. Rodgers, K. B. *et al.* A wintertime uptake window for anthropogenic CO<sub>2</sub> in the North  
355 Pacific. *Glob. Biogeochem. Cycles* **22**, GB2020 (2008).
- 356 29. Egleston, E. S., Sabine, C. L. & Morel, F. M. M. Revelle revisited: Buffer factors that  
357 quantify the response of ocean chemistry to changes in DIC and alkalinity. *Glob.*  
358 *Biogeochem. Cycles* **24**, GB1002 (2010).
- 359 30. Hauck, J. & Völker, C. Rising atmospheric CO<sub>2</sub> leads to large impact of biology on  
360 Southern Ocean CO<sub>2</sub> uptake via changes of the Revelle factor. *Geophys. Res. Lett.* **42**,  
361 2015GL063070 (2015).
- 362 31. Orr, J. C. Recent and future changes in ocean carbonate chemistry. in *Ocean*  
363 *acidification* **1**, 41–66 (2011).
- 364 32. Kerrison, P., Hall-Spencer, J. M., Suggett, D. J., Hepburn, L. J. & Steinke, M.  
365 Assessment of pH variability at a coastal CO<sub>2</sub> vent for ocean acidification studies. *Estuar.*  
366 *Coast. Shelf Sci.* **94**, 129–137 (2011).
- 367 33. Schulz, K. G. & Riebesell, U. Diurnal changes in seawater carbonate chemistry  
368 speciation at increasing atmospheric carbon dioxide. *Mar. Biol.* **160**, 1889–1899 (2013).
- 369 34. Jury, C. P., Thomas, F. I. M., Atkinson, M. J. & Toonen, R. J. Buffer Capacity, Ecosystem  
370 Feedbacks, and Seawater Chemistry under Global Change. *Water* **5**, 1303–1325 (2013).

371

372

373

374

375

376

377

378

379

380

381

382

383

384

385 **Acknowledgements**

386

387 This study was funded by the H2020 CRESCENDO grant (ref 641816) and the ERC  
388 IMBALANCE-P synergy grant (ref 610028). We acknowledge the World Climate Research  
389 Programme's Working Group on Coupled Modelling, which is responsible for CMIP. For CMIP  
390 the US Department of Energy's Program for Climate Model Diagnosis and Intercomparison  
391 provided coordinating support and led the development of software infrastructure in  
392 partnership with the Global Organisation for Earth System Science Portals. To analyse the  
393 CMIP5 data, this study benefited from the IPSL Prodiguer-Ciclad facility, which is supported  
394 by CNRS, UPMC, Labex L-IPSL which is funded by the ANR (ref ANR-10-LABX-0018) and by the  
395 European FP7 IS-ENES2 project (ref 312979). We thank B. Le Vu for preliminary discussions.

396

397 **Author contributions**

398

399 Both authors conceived this study, J.O. produced the derived variables, and both authors  
400 performed the analysis and wrote the manuscript, with L.K. leading the process.

401

402 **Additional information**

403

404 Correspondence and requests for materials should be addressed to L.K.

405

406 **Competing financial interests**

407

408 The authors declare no competing financial interests

409

410

411

412

413

414

415

416

417

418

419

420

421

422

423

424

425

426

427

428

429

430

431

## 432 **Methods**

433

### 434 ***Earth System Models***

435

436 Monthly surface-ocean carbonate chemistry fields were computed from monthly output of 9  
437 CMIP5 models (Table S1) from prognostic fields for total alkalinity, dissolved inorganic  
438 carbon, temperature, salinity, and total dissolved inorganic phosphorus and silicon.  
439 Calculations were made offline using the *mocsy* package and the equilibrium constants  
440 recommended for best practices<sup>35</sup>. Output fields were regridded to a regular 1° x 1° regular  
441 grid to facilitate multi-model intercomparison. All quoted error bars represent one standard  
442 deviation of the multi-model mean.

443

### 444 ***Model evaluation***

445

446 CMIP5 seasonal climatologies constructed from 1995-2004 model output years were  
447 compared against the Takahashi et al., 2014 (ref. <sup>6</sup>) observational climatologies of [H<sup>+</sup>], pH,  
448 *p*CO<sub>2</sub> and Ω<sub>arag</sub> (Supplementary Figs. 1-6). Model output was regridded to the Takahashi 4° x  
449 5° grid with the same ocean mask applied. The models generally capture the zonal-mean  
450 patterns of seasonality for observed climatologies of [H<sup>+</sup>], pH, *p*CO<sub>2</sub> and Ω<sub>arag</sub>.  
451 The multi-model ensemble encompasses the observed seasonal variance for Ω<sub>arag</sub> yet  
452 overestimates the seasonal variance of [H<sup>+</sup>] and *p*CO<sub>2</sub> (Supplementary Figs. 1-2). This  
453 overestimation is driven by the zonal-mean component of seasonal variance (Supplementary  
454 Figs. 1-2). Across all carbonate chemistry variables, models have high correlation coefficients  
455 for the zonal-mean component of seasonal variability and relatively low correlation  
456 coefficients for the zonal-anomaly component of seasonal variability. Model performance is  
457 generally best in the subtropics and worst in the Southern Ocean with respect to both [H<sup>+</sup>]  
458 and Ω<sub>arag</sub> (Supplementary Figs. 3-6). Yet in the Southern Ocean, the data used to construct  
459 the climatologies are typically summer biased.

460

### 461 ***Idealised simulations***

462

463 Three out of the 9 models also ran idealised simulations that allowed us to separate the  
464 geochemical effect from the CO<sub>2</sub> increase from the radiative forcing effect of the same CO<sub>2</sub>  
465 increase. More precisely, we used results from three CMIP5 experiments: 1pctCO<sub>2</sub>,  
466 *esmFixClim1* and *esmFdbk1*. Although these simulations are not directly comparable to  
467 those with the RCP8.5 scenario due to different simulation lengths and atmospheric CO<sub>2</sub>  
468 concentrations, they provide the only means of separating the ultimate geochemical and  
469 radiative drivers of seasonality change. In the 1pctCO<sub>2</sub> simulations, the atmospheric CO<sub>2</sub>  
470 concentration increases from 280 ppm by 1 % per year reaching a doubling (2xCO<sub>2</sub>) after 70  
471 years (560 ppm) and quadrupling (4xCO<sub>2</sub>) after 140 years. In the *esmFixClim1* simulations,  
472 the atmospheric CO<sub>2</sub> concentration follows that of the 1pctCO<sub>2</sub> simulations while the  
473 radiative module of each model experiences a constant atmospheric CO<sub>2</sub> concentration of  
474 280 ppm. Conversely, in the *esmFdbk1* simulations, the atmospheric CO<sub>2</sub> concentration is  
475 held constant at 280 ppm but the radiative module of each model experiences the same CO<sub>2</sub>  
476 concentration as the 1pctCO<sub>2</sub> simulations. The mean response of the models in the 1pctCO<sub>2</sub>  
477 simulations is similar spatially to that of the multi-model ensemble in RCP8.5 simulations  
478 (Figs. 3, 4). This confirms that atmospheric CO<sub>2</sub> emissions are the driver of patterns of

479 carbonate chemistry seasonality change and validates the use of the esmFixClim1 and  
480 esmFdbk1 simulations to partition the radiative and geochemical influences of CO<sub>2</sub>. It should  
481 be noted that there are limited increases in ocean temperatures in the esmFixClim1  
482 simulations that result from changes associated with the terrestrial biosphere, for which  
483 elevated CO<sub>2</sub> reduces stomatal conductance, which in turn drives greater surface sensible  
484 heat fluxes and thus slight increases in temperatures<sup>36</sup>.  
485

### 486 ***Taylor-series deconvolution***

487  
488 The first-order Taylor-series deconvolution was performed for [H<sup>+</sup>] and Ω<sub>arag</sub> independently  
489 with output from the RCP8.5 simulations (eqn. 2). The partial differential terms were  
490 estimated numerically using the *mocsy* package and ΔT, ΔC<sub>T</sub>, ΔA<sub>T</sub> and ΔS represent the  
491 change in input variables synchronous with Δy. This approach reproduces the changes in the  
492 seasonal amplitude of each of the derived variables [H<sup>+</sup>] and Ω<sub>arag</sub> to within much less than 1  
493 % as shown in Figure S9. With the exception of the very high latitudes, the deconvolution  
494 was broadly consistent across the multi-model ensemble. The zonal-mean influence of the  
495 different terms is given in the supplementary material for the representative GFDL-ESM2M  
496 model (Supplementary Figs. 9-11).  
497

### 498 ***Data availability***

499  
500 All the CMIP5 ESM model data are available via the Earth System Grid Federation (ESGF). The  
501 derived data that support the findings of this study are available from the corresponding  
502 author upon request.  
503

### 504 ***References***

- 505  
506  
507 35. Dickson, A. G., Sabine, C. L. & Christian, J. R. Guide to Best Practices for Ocean CO<sub>2</sub>  
508 Measurements. (North Pacific Marine Science Organization, 2007).  
509  
510 36. Sellers, P. J. *et al.* Comparison of Radiative and Physiological Effects of Doubled  
511 Atmospheric CO<sub>2</sub> on Climate. *Science* **271**, 1402–1406 (1996).  
512  
513  
514  
515